Coherent Diffraction Imaging of Nanoscale Strain Evolution in a Single Crystal under High Pressure

Wenge Yang[1*], Xiaojing Huang[1], Ross Harder[2], Jesse N. Clark[3], Ian K. Robinson[3,4]
and Ho-kwang Mao[1,5]

[1]High Pressure Synergetic Consortium, Geophysical Laboratory, Carnegie Institution of Washington, Argonne, IL 60439, USA
[2]Advanced Photon Source, Argonne National Laboratory, Argonne, IL 60439, USA
[3]London Centre for Nanotechnology, University College London, London WC1E 6BT, UK
[4]Research Complex at Harwell, Didcot, Oxfordshire OX11 0DE, UK
[5]Geophysical Laboratory, Carnegie Institution of Washington, Washington, DC 20015, USA

The evolution of internal strain under high pressure fundamentally alters the physical property, structural stability, phase transition and deformation mechanism of materials. Until now, only strain distributions averaged over many crystal grains have been studied. Bragg coherent X-ray diffraction imaging is highly sensitive to the internal strain distribution of individual crystals but requires coherent illumination, which can be compromised by the complex sample environment needed for high-pressure study. Here we report the successful de-convolution of these effects to reveal the 3D strain distribution inside a 400 nm gold single crystal during compression within a diamond anvil cell. The 3D morphology and evolution of the strain under pressures up to 6.4 GPa were obtained with better than 30 nm spatial resolution. In addition to providing a new approach for high pressure nanotechnology and rheology studies, we draw fundamental conclusions about the origin of the anomalous compressibility of nanocrystals.

*Correspondence and requests for materials should be addressed to W.Y. (e-mail: wyang@ciw.edu)

The elastic strain of a material is formally described as the derivative of the displacement of atoms from their perfect lattice locations. It can arise as residual strain following certain processes as mechanical deformation, phase transitions, crystal growth or formation of defects. Strain can also be induced by external pressure, electric or magnetic fields or by temperature through differential thermal expansion. *In-situ* study of the strain evolution under high pressure provides key information for fundamental physics understanding and engineering materials development at extreme conditions[1]. This is made possible for X-ray diffraction, because of its deep penetration, by means of the Diamond Anvil Cell[2].

Conventional x-ray diffraction resolves strain either as an average over many grains in powder diffraction[3] or one grain at a time in single crystal diffraction[4]. The recent developed depth-resolved x-ray diffraction technique can provide internal strain distribution along the beam penetration direction with about 1 μm point-to-point spatial resolution, providing crystal orientation and strain information for mesoscale structural analysis[5]. To study nanometer-sized grains, a much higher spatial resolution probe is required. The Bragg coherent X-ray diffraction imaging (CXDI) technique is a promising tool to probe the internal strain distribution of individual nanometer-sized single crystals[6]. Coherence is a property that can be imposed on an X-ray beam by setting an entrance slit smaller than the transverse coherence length. X-ray beams generated by 3rd-generation sources of Synchrotron Radiation (SR) using undulators have practical levels of coherent flux in the range of 10^9 photon/sec. As the coherent x-rays pass through a distorted crystal, both the scattering intensity and phase will be affected. Bragg CXDI operates by inverting 3D diffraction patterns in the vicinity of Bragg peaks to real-space images using phase retrieval algorithms[7]. In the resulting images, the reconstructed magnitude represents the electron density of the crystal, while the obtained phases are attributed to lattice distortions projected onto the Bragg direction. CXDI is also called lensless microscopy, because it uses the least optical components possible in the beam path from source to detector to preserve the transverse coherence. So long as the beam is also sufficiently monochromatic, it will then have full spatial coherence[8].

In the case of partially coherent illumination, the recorded intensity is given by[9-11]

$$\boldsymbol{I}_{pc}(\boldsymbol{q}) = \int \left(\int \psi(\boldsymbol{r})\psi(\boldsymbol{r}+\boldsymbol{x})d\boldsymbol{r} \right) \gamma(\boldsymbol{x}) \cdot \boldsymbol{e}^{-i2\pi x\cdot q} d\boldsymbol{x} = \left|\hat{\psi}(\boldsymbol{q})\right|^2 \otimes \hat{\gamma}(\boldsymbol{q}) = \boldsymbol{I}_c(\boldsymbol{q}) \otimes \hat{\gamma}(\boldsymbol{q}) \qquad \textbf{(1)}$$

where $\gamma(\boldsymbol{x})$ and $\hat{\gamma}(\boldsymbol{q})$ are the so-called mutual coherent function (MCF) and its Fourier transform, and $\boldsymbol{x}$ is the separation in the plane of the sample. The scalar wavefield $\psi(\boldsymbol{x})$ and scalar diffracted wavefield ⍰($\boldsymbol{q}$) are complex. Unlike the direct phase retrieval method used for ideal full coherent diffraction case, both the wavefield and MCF are updated at each step of the iterative phase retrieval calculation until both quantities converge. This method has been successfully demonstrated for Au nanocrystals similar to those used in this work[10]. The de-convolution of the MCF turned out to be crucial to the full coherent imaging of our studies presented here.

For *in-situ* static high pressure study, the diamond anvil cell (DAC) is the most common apparatus to generate pressure up to multi-Mega bar[2]. The sample is inserted between two anvils made of diamond inside the hole of a gasket and surrounded by a pressure transmitting medium. X-rays need to pass through either the diamond anvils or the gasket and the pressure medium, all of which can significantly affect the wave front of the beam. Especially when these components are refractive, this could have a deleterious impact on the ability to obtain an image by CXDI, because it restructures both the beams entering and leaving the sample environment. Strictly, the degree of coherence of the beam, described by the mutual coherent function (MCF) is determined by the undulator SR source alone and should not be affected by this inadvertent optical distortion[9]. However, if the optical distortion is not too strong, its effect can be folded in with the pre-existing MCF of the source to make an effective MCF with smaller coherence lengths. We can then use the method of Clark et al. (ref. 10) to de-convolute the observed diffraction patterns and obtain both the 3D morphology and phase distribution of the studied crystal. Strain sensitivity better than $1\text{x}10^{-4}$ and spatial resolution better than 30 nm can be achieved.

The mechanical properties of nanoscale gold particles have attracted considerable interest for tailoring the properties of molecular electrodes, nanoscale coatings and advanced engineering materials[12-14]. A recent high-pressure study on 30 nm gold particles[15] has shown they have 60% higher stiffness compared with micron-size counterparts. Our CXDI method can examine the distribution of strains *within* a nanocrystal to understand where this enhanced stiffness is located.

Hence exploring the mechanical response of gold crystals under high pressure at nanometer scale can impact both fundamental physics and applied sciences. When a gold crystal is under a quasi-hydrostatic pressure in a DAC, any shear stress will create a boundary condition to affect the internal strain distribution, which could create lattice distortions, morphology change and plastic flow as the applied external pressure increases. In this letter, we report the strain and morphology evolution on a single gold nanograin as the pressure change to gain insight on the possible nanoscale mechanism of its high pressure response.

The schematic of the experimental setup is shown in Fig. 1. 3D diffraction patterns from the same gold crystal in a diamond anvil cell were collected at several pressure conditions up to 6.4 GPa (see the method section). In order to reduce the systematic effects of wavefront distortion, typically 5-8 repeated scans were collected at each pressure point, under slightly different alignment conditions, and averaged together. The diffraction data were inverted using phase retrieval algorithms, which utilize sufficiently oversampled diffraction intensities to recover the unmeasured phases of diffraction signal. In the reconstruction process, known information is imposed as constraints. The usual constraints are: modulus constraint which requires that the calculated Fourier intensity agrees with the measured data, and support constraint which assumes that the sample is finite and isolated from other scatters in real space. We used a reconstruction cycle with an algorithm sequence of 10 error-reduction (ER), 150 hybrid-input-output (HIO) and 40 ER. The "shrink-wrap" strategy was used to refine the crystal shape used as a support[16].

To de-convolute the influence of beam disturbance by the DAC gasket and pressure medium, modeled as a modified MCF, we used the method developed for CXDI with partial coherence[10]. The MCF is convolved with the calculated Fourier modulus before applying the modulus constraint. The unknown MCF function is updated regularly using iterative Richardson-Lucy algorithm[17,18]. The searching criterion is to minimize the variation between the measured data and the convolution of this characterization function with calculated Fourier modulus. The reconstructed images using data measured at the initial pressure 0.8 GPa with and without incoherence correction are shown in Fig. 2 (a). We found that the coherence correction gives a smoother crystal boundary and significantly improves the algorithm's convergence, as found previously by Clark[10]. The corresponding MCF function for this data set is plotted in Fig. 2 (b). The extracted MCF is a three-dimensional function which includes the transverse coherence properties in the XY-plane, perpendicular to the incident x-ray beam direction, and the temporal (or longitudinal) coherence properties related to the monochromaticity of the wavefield along its Z-direction. The effect of applying the MCF is to blur the coherent intensity from measured sample by convolving it with the Fourier transform of the MCF[9,10]. The MCF, along X, Y, and Z directions, is plotted in Fig. 2(b), from where one can see from the smooth decay of the MCF that any pair of points separated by some distance are partially coherent.

As seen in the scanning-electron microscopy (SEM) image of the gold nanoparticles in Fig. 1, the individual particles often adopt a faceted morphology, probably related to the equilibrium crystal shape at the annealing temperature. Fig. 3 displays the reconstructed results of the 400 nm crystal at 1.7 GPa. The magnitude of the reconstructed density $\psi(\boldsymbol{x})$ at its 30% isosurface is shown in Fig. 3a. The surface normal is along (111) direction, and the crystal shape shows a good three fold symmetry. We notice that all faceted surface planes can be described as either {111} or {100} crystalline planes. A tight wrap model, defined by all {111} and {100} planes, is overlaid with the 30% isosurface object in Fig. 3a. Fat and narrow arrows denote the {111} and {100} plane normal directions, respectively. The arrow labeled as red in Fig. 3(a) represents the q-vector direction of the Bragg reflection used. Fig. 3(b) and 3(c) are the top and bottom view of phase shift, respectively. The color shows the phase shift relative to the average phase of entire particle, set to zero. The phase shift color is normalized to range [-π/4, π/4]. The bottom two rows in Fig. 3 are slices through the 3D reconstructed phase object in 20 nm depth steps running from top to bottom. One can see the high strain areas are mainly located at the corners where two {111} planes and one {100} plane intersect. The interior volume is nearly strain free. Three distinguished corners marked as 1, 2 and 3 in Fig. 3(b) and (c) were selected for further quantitative strain analysis as applied pressure increases.

The Bragg CXDI measurements were performed at 0.8, 1.7, 2.5, 3.2 and 6.4 GPa on the same crystal. The reconstructed images (both top and bottom views) are shown in Fig. 4(a). The dimension of the measured crystal is about 480×380×180 nm at 0.8 GPa and shrinks a little bit as pressure increases. The noteworthy features in Fig. 4 are the morphology change and strain redistribution as pressure increases. The phase shifts as a function of pressure at the selected 3 locations are plotted in Fig. 4(b). At each selected corner region, the phase shift values within 3 ×3×3 pixel boxes around the center were taken, and the averaged values were plotted as a function of pressure in Fig. 4(b), where the maximum and minimum values in the 3×3×3 boxes were used as the error bar range, respectively. The phase value is directly connected to the local lattice displacement, thus strain, projected to the measured $\vec{q}$ direction as $\phi = \vec{q} \cdot \Delta\vec{r}$ (Ref. 6).

It is clearly seen that the strain level decreases as pressure increases while the crystal shape evolves significantly. The starting, well-faceted shape becomes smoother around the corners, which implies large plastic flow has taken place within the sample during the compression. Location 2 is anomalous: initially the strain level was relatively low at 0.8 GPa, as at 1.7 GPa, the local strain was quickly built up while a geometrically sharp corner was formed. Upon further compression, this sharp corner became rounder while the rest of the sample and strain level were decreasing quickly. For checking the overall phase shift evolution as a function of pressure, we evaluated the standard deviation of phase over the entire crystal in Fig. 4(c), where phase variation is calculated as $\phi_{\text{var}} = \sqrt{\sum_{i=1}^{N} (\phi_i - <\phi_i>)^2 / N}$. The overall trend is the average phase variation decreases with pressure.

A phase shift of 1.0 radian (about the highest phase shift measured here) corresponds to a lattice strain of ~2×10^{-4} at the edge of the crystal along the measured $\vec{q}$ vector direction. As the measured phase shift is only the projected component along the $\vec{q}$ direction, the real strain should be larger than our observation. Overall the strain sensitivity better than 1×10^{-4} is achievable.

Besides the dramatic changes at the selected corners, the overall strain evolution at the bottom of the crystal, the interface between crystal and substrate SiO_2 layer, was also significant. At 0.8 GPa, the bottom surface is nearly strain-free indicating the high temperature treatment when sample was formed has released the interface strain between gold crystal and SiO_2 surface well. As pressure increased to 1.7 GPa, strain started to build up at two areas away from the center (lower-left and upper-right). A uniform but strained distribution formed at 2.5 GPa, and a new high-strain center reemerged near the center of the bottom surface at 3.2 GPa. At the highest pressure measured in this work (6.4 GPa), the strain was largely relieved near the newly formed hole in the central part but large strain has shifted to the side (bottom and right), which counts for the increasing average phase variation in Fig. 4(c). A new sharp corner has emerged at the right side too. The missing part of electron density from the amplitude reconstruction implies the bottom of the crystal may have partially de-bonded from the substrate. Upon further compression, we noticed this crystal disappeared from the detector even after both reciprocal and real space searching, which indicated the crystal was totally de-bonded from substrate and rotated to a different orientation or moved out of the searching field.

The usual result of high pressure powder diffraction under quasi-hydrostatic conditions, is that the diffraction peaks become broader at higher pressure, suggesting a larger strain variation. From this single crystal CXDI study, we found the opposite, that the overall strain variation cross the entire crystal decreases with the applied pressure increases. This apparent discrepancy can be attributed to the fact that we examined an isolated grain in the current study, in the absence of interactions with adjacent grains.

To summary, the three-dimensional strain distributions in a ~ 400 nm gold crystal were measured with about 30 nm spatial resolution and 1×10^{-4} strain sensitivity by Bragg coherent diffraction imaging technique under an applied pressure from 0.8 GPa to 6.4 GPa in a diamond anvil cell. Once de-convoluted from a mutual coherent function, the coherent diffraction patterns were successfully reconstructed and inverted to 3D images. Upon increasing the applied pressure, some of the initial high-strain corners in the crystal shape reduce their strain level, while other areas acquire a sharper local geometry and higher local strain. Upon further pressure increases, the strain at all these locations dropped and stayed at low level. The current research for the first time demonstrates the powerful capability of Bragg CXDI to study the internal strain evolution under high pressure with 30 nm spatial resolution and strain level better than $1\text{x } 10^{-4}$, which leads to a very promising approach for *in-situ* nanoscale rheology under high pressures.

Acknowledgement. This work was supported by EFree, an Energy Frontier Research Center funded by DOE-BES under Grant number DE-SC0001057 and by the ERC “nanosculpture” advanced grant 227711. APS is supported by DOE-BES, under contract No. DE-AC02-06CH11357.

Author Contributions W.Y., I.K.R. and H.K.M. designed the project; W.Y., R.H. and I.K.R. performed the experiments; W.Y., X.H., I.K.R. and H.K.M. wrote the paper; W.Y., X.H., R.H., J.N.C. and I.K.R. analyzed the data. All the authors read and commented on the manuscript.

Methods

Experimental details. The gold nanocrystals were prepared by dewetting of evaporated gold films at a temperature just below melting[19]. A 20 nm thick gold film was deposited on silicon wafer surface. It was then annealed in air in a furnace at 1100°C for several hours. Isolated gold crystals were formed, about 300-400 nm in diameter, 200 nm in height and about 1 μm separation, with {111} 'fibre' texture. A small piece of the silicon wafer containing gold crystals was mechanically polished down to about 15 μm from the back side in order to fit in the gasket hole. A panoramic diamond anvil cell (DAC) with a pair of 300 μm culet size diamond anvils was used for the *in-situ* high pressure study. A Beryllium gasket was pre-indented to 40 μm thick and a 150 μm diameter hole was drilled in the center to host the silicon wafer and a small ruby sphere. A mixture of Methanol and Ethanol (4:1) was used as pressure transmitting medium. The pressures were monitored from the Ruby fluorescence shift[20].

The Bragg CXDI experiment was performed at Beamline 34-ID-C of the Advanced Photon Source, Argonne National Laboratory. A coherent 10.8 keV X-ray beam was selected by a silicon (111) double crystal monochromator, and focused to ~ 1.5 μm FWHM in diameter with a pair of Kirkpatrick-Baez mirrors. The studied crystal inside the DAC was aligned to the rotation center of the diffractometer. An X-ray sensitive charge-coupled device (CCD) was positioned at the desired diffraction angle, 1m from the sample. The off-specular (111) reflection of the gold crystals was chosen to allow separation of the signals from multiple crystals in the beam. In order to follow the same particle after changing pressure, a local search in reciprocal space was performed to pick an isolated single crystal within half a degree along the 2 theta arc to guarantee only one (111) reflection in this region. Once the particular grain was chosen, we also moved the sample stage in the plane perpendicular to the incident beam to ensure no similar oriented crystals were found within 3 times the beamsize (~ 5 microns). To measure its full 3D diffraction pattern, the crystal was rotated by 0.4 degree with 0.01 degree step size. At each rotation angle, a 2D frame of the 3D far-field diffraction pattern was recorded by the CCD placed 1 m away from the sample. By stacking all these 2D diffraction frames together, a complete 3D diffraction pattern was obtained, from which real-space images can be reconstructed, solving the phase problem by oversampling and a support constraint[6]. An online ruby system was installed above the DAC to monitor the pressure *in situ*, which allows one to change pressure without taking the cell off the sample stage.

References:

1. Bridgman, P. W. The Physics of high pressure. London, G. Bell (1949).
2. Mao, H. K., Wu, Y., Chen, L. C., Shu, J. F., & Jephcoat, A. P. Statis compression of iron to 300 GPa ad Fe0.8Ni0.2 alloy to 260 GPa: implications for composition of the core. J. Geophys. Res. 95, 737-742 (1990).
3. Langford, J.I., & Louer D. Powder diffraction. Rep. Prog. Phys., 59, 131- 234(1996).

4. Margulies L., Lorentzen T., Poulsen H. F., & Leffers T. Strain tensor development in a single grain in the bulk of a polycrystal under loading. Acta Materialia 50, 1771-1779 (2002).
5. Larson, B. C., Yang, W., Ice, G. E., Budai, J. D., & Tischler J. Z. Three dimensional x-ray structural microscopy with submicrometre resolution. Nature 415, 887-890 (2002).
6. Robinson I. K., & Harder R. Coherent x-ray diffraction imaging of strain at the nanoscale. Nature Materials 8, 291-298 (2009).
7. Pfeifer, M. A., Williams, G. J., Vartanyants, I. A., Harder, R. & Robinson, I. K. Three-dimensional mapping of a deformation field inside a nanocrystal. Nature **442,** 63–66 (2006).
8. Goodman, J. W. Statistical Optics. New York: Wiley (1985).
9. Nugent, K.A. Partially coherent diffraction patterns and coherence measurement. J. Opt. Soc. Am. 8, 1574-1579 (1991).
10. Clark, J., Robinson, I. K., Huang, X. J., & Harder, R. Three-dimensional partially coherent diffraction imaging. (to be published, 2012).
11. Vartanyants, I. A. & Robinson, I. K. Partial coherence effects on the imaging of small crystals using coherent X-ray diffraction. J. Phys. Condens. Matter **13,** 10593–10611 (2001).
12. Liang, W., Shores, M., Bockrathm M., Long, J.R., & Park, H. Kondo resonance in a single-molecule transistor. Nature 417, 725- 719 (2002).
13. Eah S.K. A very large two-dimensional superlattice domain of monodisperse gold nanoparticles by self-assembly. J. Mater. Chem. 21, 16866-16868 (2011).
14. Hodge, M., Hayes, J. R., Caro, J. A., Biener, J., & Hamza, A. V. An Overview on the Characterization and Mechanical Behavior of Nanoporous Gold. Advanced Engineering Materials **8**, 853- 857(2006).
15. Gu, Q. F., Krauss, G., Steurer W., Gramm F., & Cervellino A. Unexprected high stiffness of Ag and Au nanoparticles. Phys. Rev. Lett. 100, 045502 (2008).
16. Marchesini, S., *et al*. X-ray image reconstruction from a diffraction pattern alone. Phys. Rev. B 68. 140101 (2003).
17. Richardson, W. Bayesian-based iterative method of image restoration. J. Opt. Soc. Am. 62, 55-59 (1972).
18. Lucy, L. Iterative technique for rectification of observed distributions. Astro. J. 79, 745-754 (1974).
19. Robinson, I. K., Vartanyants, I., Williams, G., Pfeifer, M., & Pitney, J. Rconstruction of the shapes of gold nanocrystals using coherent x-ray diffraction. Phys. Rev. Lett. 87, 195505 (2001).
20. Mao H. K., Xu, J., & Bell P. M. Calibration of the Ruby pressure gauge to 800 kbar under quasi-hydrostatic conditions. J. Geophys. Res. 91, 4673-4676 (1986).

Figure Captions:

Figure 1. Overall schematic of the experimental setup. A large opening panoramic diamond anvil cell is used to compress the studied crystal, positioned at the rotation center of the diffractometer. An X-ray sensitive CCD is placed at 1 m away to collect far-field diffraction patterns. The insert SEM picture shows typical gold nanoparticles distributed on a silicon substrate. The zoomed-in figure of the DAC shows the sample environment.

Figure 2. Impact of the mutual coherent function (MCF) on the reconstructed images at 0.8 GPa pressure. The reconstructed amplitude plots at top, bottom and side views with (left) and without (right) MCF correction (a), and the corresponding line profiles along x, y, z directions of the MCF (b).

Figure 3. 3D amplitude and strain distribution of the gold crystal at 1.7 GPa. (a) 30% isosurface of the reconstructed amplitude superimposed with a model of the possible {111} and {100} crystal planes. The fat and narrow arrows represent {111} and {100} plane normal directions, respectively and the one (111) used for the measurement was marked in red. (b), (c) are the top and bottom view of phase shift distribution pasted on the 30% isosurface plot. Three strain distinguished locations numerically labeled are chosen for quantitative measurement as a function of pressure. (d) 3D phase distribution at different slicing depths spaced apart by 20 nm steps from top to bottom of the crystal. The color scale is used to show the relative phase shift and normalized to range [-π/4, π/4].

Figure 4. Phase distribution as a function of applied pressure (0.8 GPa to 6.4 GPa) from the top and bottom view (a). The quantitative phase shift values at locations 1-3 labeled in Fig. 3 and the phase variation over entire crystal are plotted in (b) and (c) as a function of pressure.

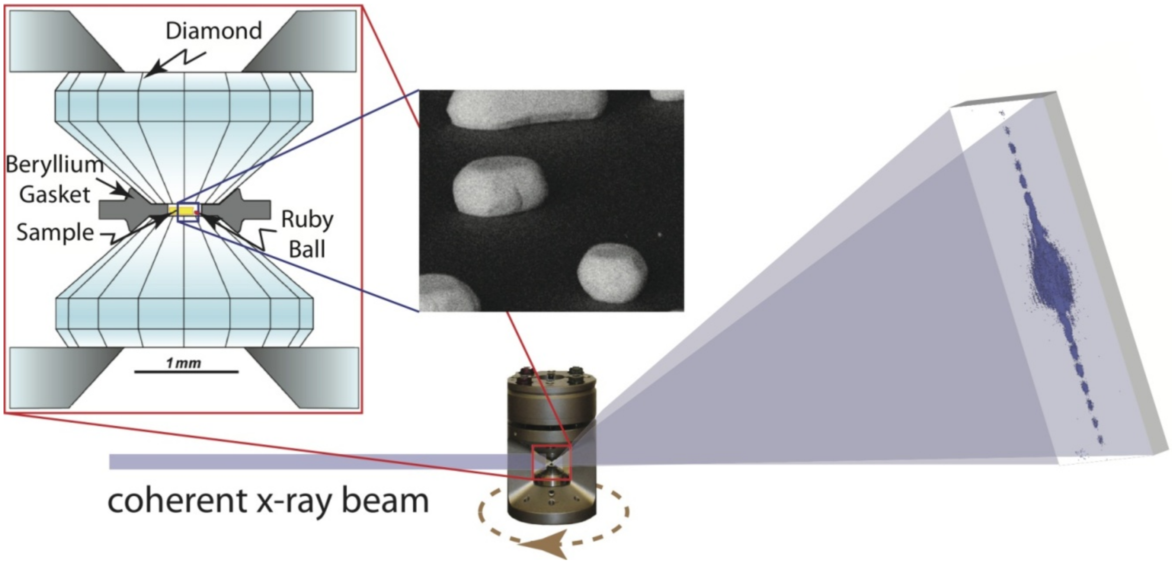

Fig. 1 Yang et al.

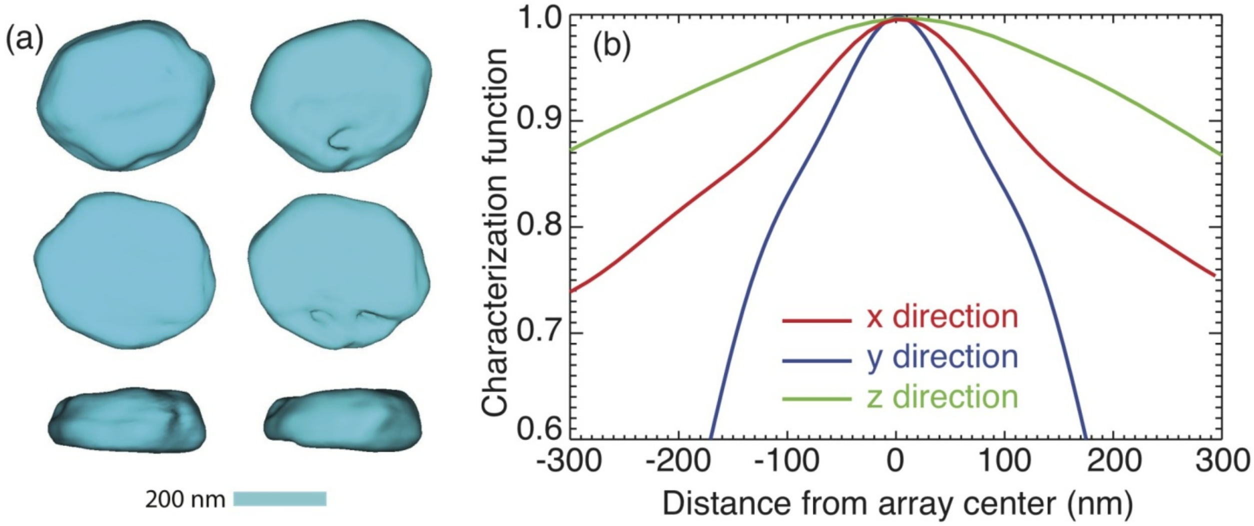

Fig. 2 Yang et al.

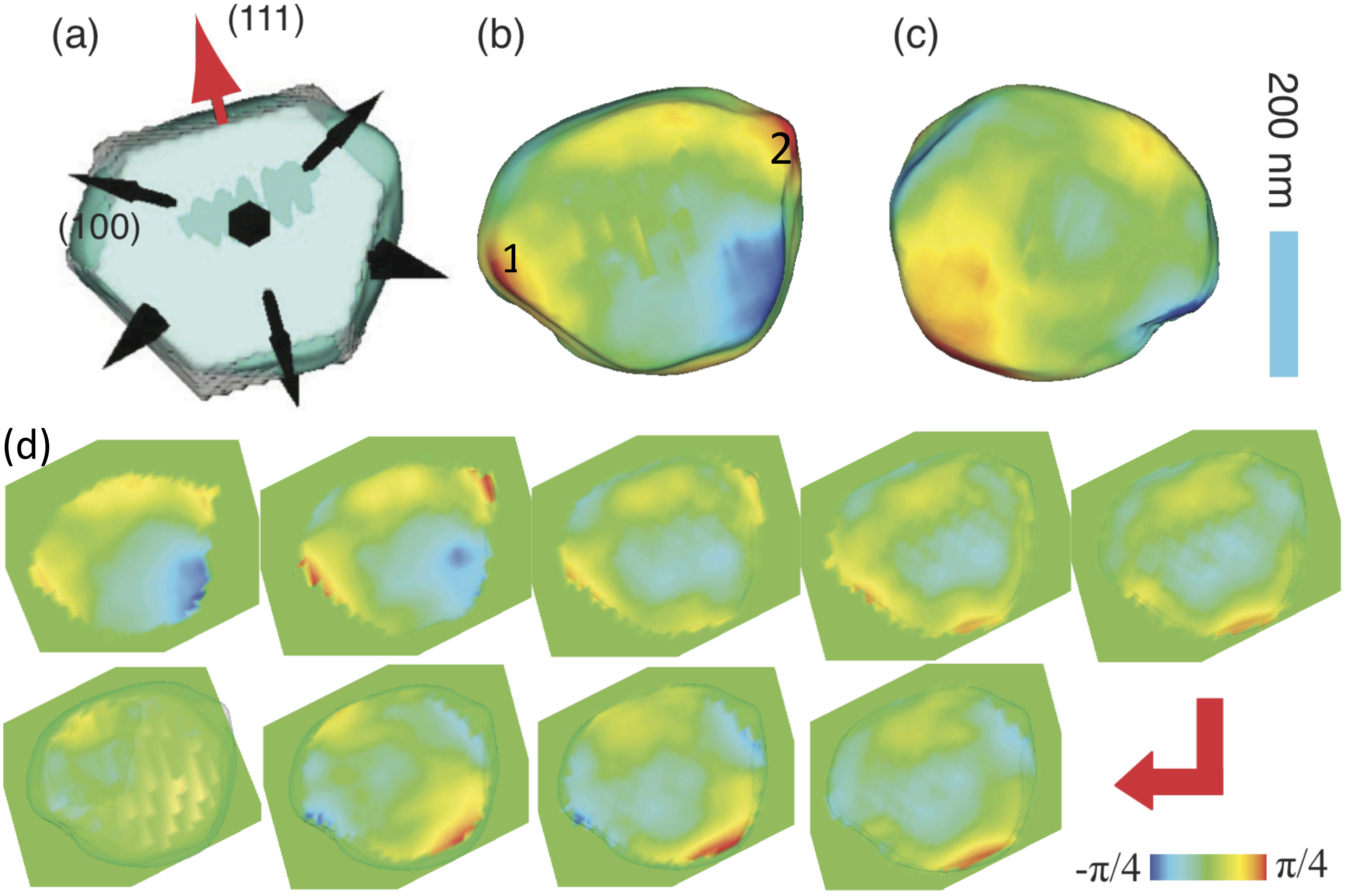

Fig. 3 Yang et al.

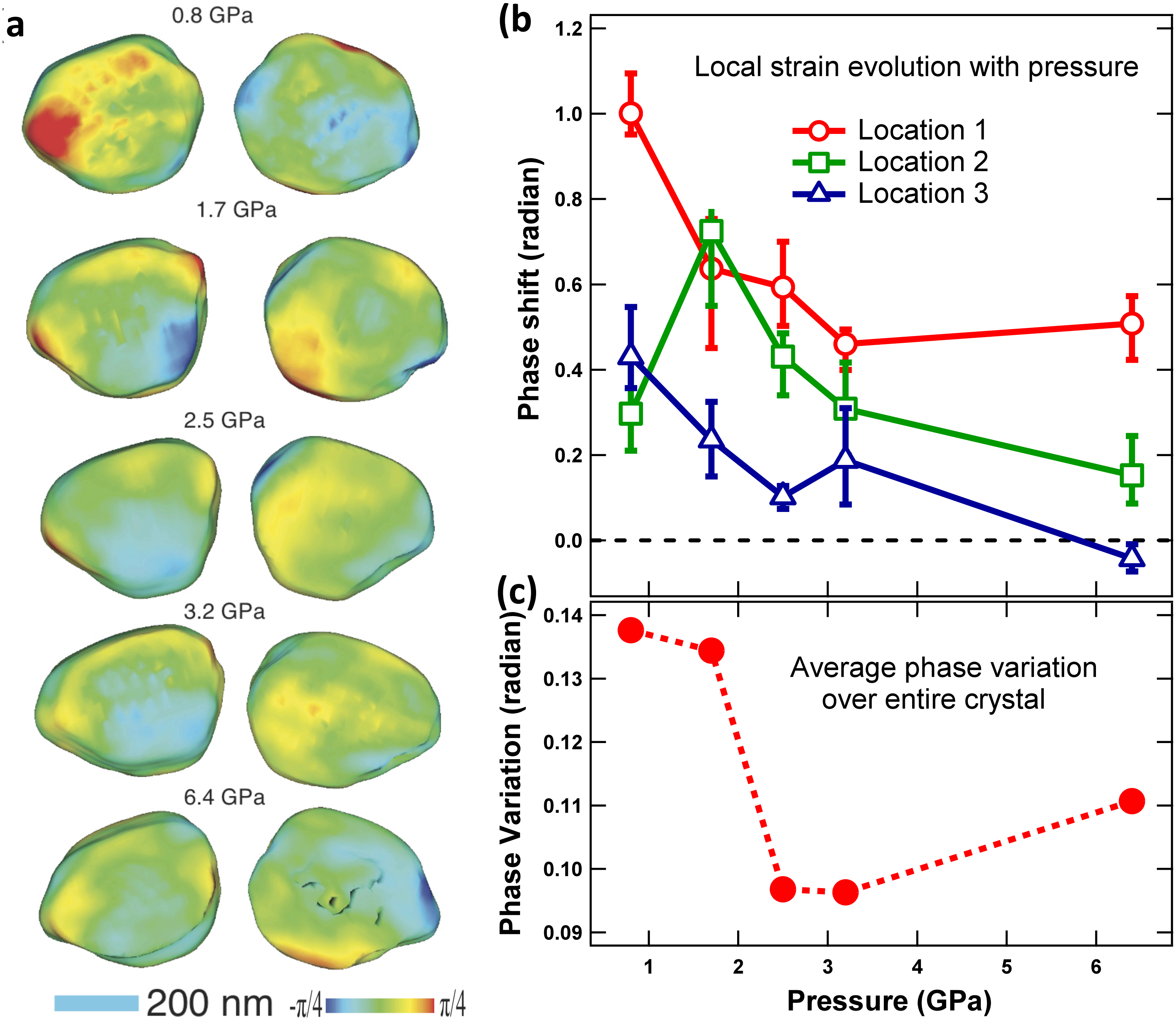
a
0.8 GPa
1.7 GPa
2.5 GPa
3.2 GPa
6.4 GPa
200 nm
-π/4
π/4
(b)
Local strain evolution with pressure
Location 1
Location 2
Location 3
Phase shift (radian)
1.2
1.0
0.8
0.6
0.4
0.2
0.0
(c)
Average phase variation over entire crystal
Phase Variation (radian)
0.14
0.13
0.12
0.11
0.10
0.09
1
2
3
4
5
6
Pressure (GPa)

Fig. 4 Yang et